Functionalized Nanoporous Gold Leaf Electrode Films for the Immobilization of Photosystem I

Peter N. Ciesielski,[†,‡] Amanda M. Scott,[‡] Christopher J. Faulkner,[‡] Brad J. Berron,[‡] David E. Cliffel,[§] and G. Kane Jennings[‡,*]

[†]Interdisciplinary Materials Science Program, and [§]Department of Chemistry, Vanderbilt University, Nashville, Tennessee 37240 and [‡]Department of Chemical and Biomolecular Engineering, Vanderbilt University, Nashville, Tennessee 37235

ABSTRACT Plants and some types of bacteria demonstrate an elegant means to capitalize on the superabundance of solar energy that reaches our planet with their energy conversion process called photosynthesis. Seeking to harness Nature's optimization of this process, we have devised a biomimetic photonic energy conversion system that makes use of the photoactive protein complex Photosystem I, immobilized on the surface of nanoporous gold leaf (NPGL) electrodes, to drive a photoinduced electric current through an electrochemical cell. The intent of this study is to further the understanding of how the useful functionality of these naturally mass-produced, biological light-harvesting complexes can be integrated with nonbiological materials. Here, we show that the protein complexes retain their photonic energy conversion functionality after attachment to the nanoporous electrode surface and, further, that the additional PSI/electrode interfacial area provided by the NPGL allows for an increase in PSI-mediated electron transfer with respect to an analogous 2D system if the pores are sufficiently enlarged by dealloying. This increase of interfacial area is pertinent for other applications involving electron transfer between phases; thus, we also report on the widely accessible and scalable method by which the NPGL electrode films used in this study are fabricated and attached to glass and Au/Si supports and demonstrate their adaptability by modification with various self-assembled monolayers. Finally, we demonstrate that the magnitude of the PSI-catalyzed photocurrents provided by the NPGL electrode films is dependent upon the intensity of the light used to irradiate the electrodes.

KEYWORDS: biomimetic · Photosystem I · nanoporous gold leaf · self-assembled monolayer · biocatalysis · photoelectrochemistry

Photosystem I (PSI),[1] a supramolecular protein complex found within the thylakoid membrane of green plants and cyanobacteria, is one of the fundamental biochemical machines responsible for Nature's 90 TW (1 TW = 10^{12} W) solar energy conversion process known as photosynthesis.[2] PSI is an optimized nanoscale energy conversion device that coordinates a system of chlorophylls within its protein scaffolding to harvest energy from incident photons. This energy is used to initiate a charge separation within the protein by promoting an electron in the P700 reaction center to an excited state, after which the electron quickly transfers down a pathway of conjugated π-orbitals to an iron−sulfur complex at the opposite side of the protein where it becomes accessible for the reduction of other chemical species. In Nature, this photoinduced charge separation occurs within picoseconds, at a rate 100 times faster than that achieved by a silicon diode, and with a quantum efficiency near unity.[3] Recent studies have successfully demonstrated that this protein's remarkable functionality can be accessed in both solid-state nanoelectronic[4−8] and "wet" photoelectrochemical devices.[9,10]

Gold surfaces are ideal substrates for the bottom-up assembly of such devices, particularly in electrochemical applications, because of gold's broad potential window and the ease by which it is modified with various ω-terminated alkyl thiols to provide a versatile array of functional surfaces. Previous studies have demonstrated how careful selection of the terminal functional groups of SAMs on gold can be used to tune the surface energy,[11] provide a substrate for biological macromolecules,[12,13] or serve as polymerization initiators.[14−16] For many of these applications, including photoelectrochemical cells, the performance of thin films can be favorably altered by translation from a flat, two-dimensional surface to a three-dimensional architecture with nanoscale features,[17] which can both increase the available surface area and add infrastructure to the system. Several routes to achieve such surfaces patterned with columns,[18,19] tubes,[20] and pores[21] have been described previously; for applications where uniform features are not required but a high surface area is still desirable, gold nanoparticles can be deposited.[9,22] An alternative to the aforementioned techniques is offered by nanoporous gold leaf (NPGL), a free-standing mesoporous thin film that results from selectively dissolving silver

*Address correspondence to kane.g.jennings@vanderbilt.edu.

Received for review June 18, 2008 and accepted November 03, 2008.

Published online November 17, 2008.
10.1021/nn800389k CCC: $40.75

atoms from commercially available Ag−Au alloyed leaf in concentrated nitric acid.[23] This fabrication process is ideal for many applications because it efficiently incorporates inexpensive materials that are convenient for rescaling, and it can be performed under ambient conditions without the need for sophisticated processing equipment.[24]

In this article, we report the fabrication and characterization of electrode films in which NPGL is attached to planar gold and glass supports. The resulting NPGL electrode films are ultimately intended to provide a substrate for the attachment of PSI to impart photonic energy conversion capabilities to the electrode, and the surface area enhancement provided by the mesoporous network of the NPGL is expected to accommodate a greater number of PSI complexes per geometric area than a planar electrode. Previously, Terasaki *et al.* have demonstrated that a high surface area electrode prepared by gold nanoparticle deposition allowed a higher number density of PSI complexes on the electrode surface, resulting in an increased photocurrent response when compared to a planar electrode in the same electrochemical system.[9] NPGL electrode films provide several advantages to nanoparticle aggregate electrodes in that they provide better lateral conductivity and offer more control over feature size, rendering a greater percentage of the electrode surface area accessible to both PSI and the external circuit. Here, we report a PSI-catalyzed photocurrent enhancement contributed by an increase in PSI/electrode interfacial area and present evidence of the successful integration of functional PSI complexes into a scalable NPGL architecture fabricated from a material that costs ~6 cents/cm^2 of geometric surface area. We have demonstrated, through control over the NPGL feature size and modification of its surfaces, that this nonbiological system may be adapted to better interface with the functionality of these vastly abundant light-harvesting complexes.

Nanoporous Gold Leaf Electrode Fabrication. We have developed a simple electrode fabrication scheme (Figure 1) with several adaptations to the technique developed by Ding *et al.* that makes use of a graphite roller.[23] First, the as-received gold/silver leaf was cut into portions slightly larger than the final desired sample size to allow the NPGL to completely cover the substrate surface. Next, tweezers were used to gently place the leaf on a glass microscope slide, and the slide was slowly dipped into a beaker of concentrated nitric acid, causing the leaf to float at the air−acid interface (Figure 1a). As the leaf floated freely on the surface of the acid (Figure 1b), the glass slide was removed. After the dealloying had proceeded for the desired time, the leaf was removed from the acid with a glass slide by first dipping the slide into the beaker at an angle approximately 20° from the surface normal, positioning it beneath the

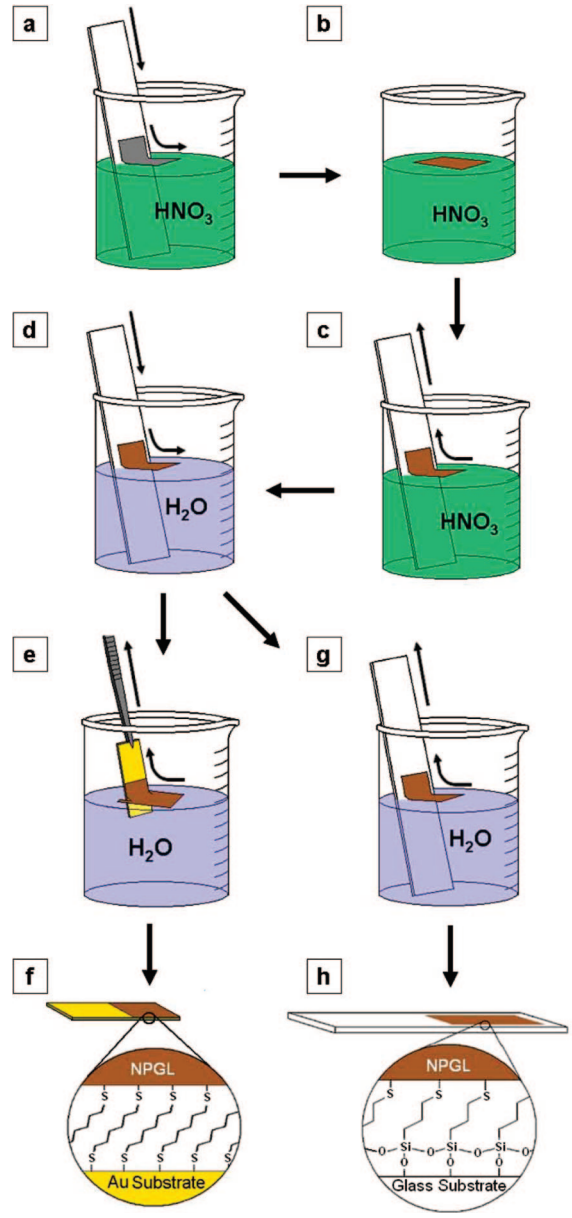

Figure 1. NPGL electrode fabrication scheme. (a) Gold−silver leaf is transferred from a glass slide to the surface of concentrated nitric acid. (b) The leaf is allowed to float on the surface of the nitric acid for a desired time during which the silver is dealloyed. (c) The dealloyed leaf is removed from the surface of the nitric acid using a glass slide. (d) The leaf is transferred to the surface of deionized water for rinsing. (e) The leaf is removed from the air−water interface with a gold substrate (on a silicon support) modified with 1,6-hexanedithiol. (f) Free thiol groups secure the NPGL onto the surface of the substrate. (g) For attachment to glass substrates, a glass slide modified by mercaptopropyltrimethoxysilane is used to remove the leaf from the water after the rinsing step. (h) Free thiols of the silane monolayer bond to the NPGL.

NPGL, and then gently withdrawing it. As the slide was removed, the free-floating leaf adhered smoothly to the surface (Figure 1c), and it was then transferred to a beaker of deionized water (Figure 1d) where it was again floated for rinsing. The leaf was removed from the air−water interface with a precut portion of a gold-

coated silicon wafer (Figure 1e) that was premodified with 1,6-hexanedithiol; as the sample was left to dry, the free thiols on the surface of the SAM bonded to the NPGL surface, fastening it firmly to the planar gold substrate (Figure 1f). This technique was adapted to attach NPGL to glass surfaces as well; the attachment was achieved by using a glass slide premodified with 3-mercaptopropyltrimethoxysilane to remove the NPGL from the air−water interface (Figure 1g,e) after the rinsing step. In both cases, evidence of the adhesion to the substrate was visually observable and appeared as a front of slightly lighter-colored NPGL propagating down the sample as the water was pushed away from the surface. This electrode fabrication scheme extends the innovative work described by Ding and Erlebacher[23] to a scalable, cost-effective means to achieve high-surface-area gold substrates with nanoscale features using techniques and materials that are easily accessible.

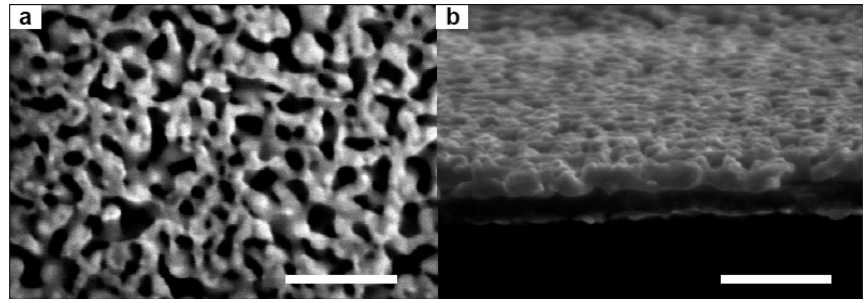

Figure 2. Scanning electron microscopy images of an NPGL electrode film on a Au support. (a) Plan view of electrode surface, scale bar 300 nm. (b) Cross section of electrode surface, scale bar 300 nm.

Scanning electron microscopy (SEM) images of an electrode surface with a dealloying time of approximately 3 h (Figure 2) reveal that the mesoporous structure of the NPGL was preserved after the leaf was attached to the flat surface of the gold substrate. The obvious contrast difference between the bright NPGL layer and the darker underlying flat gold layer shown in the cross-sectional image (Figure 2a) can be accredited to the relative ease by which secondary electrons escape the highly porous structure on the surface. The plan view image (Figure 2b) reveals that the majority of the pores have diameters between 50 and 100 nm, but some of the smallest pores have diameters of less than 30 nm. Approximating a PSI complex as an oblate spheroid with major and minor axes of 14 and 10 nm, respectively,[25] we postulate that the majority of the pores are of adequate dimensions to allow multiple PSI complexes to attach to the interior surfaces; however, some of the smaller pores could likely be filled or effectively "clogged" by a single PSI, rendering the underlying surface area inaccessible.

Electrode Surface Area Enhancements as Determined by Cyclic Voltammetry. Underpotential deposition (UPD) of silver ions from a sulfuric acid solution was performed to determine the extent to which the enhanced surface area of the newly fabricated electrode was electronically accessible and hence suitable for additional electrochemical applications. Figure 3 shows the cyclic voltammograms (CVs) of NPGL-modified electrodes created by various dealloying times, as well as a planar gold electrode plotted on the same axes for comparison. The cathodic (positive) current peaks are due to the reduction of silver ions from solution, resulting in their deposition onto the electrode surface to form a submonolayer of silver atoms. Similarly, the anodic (negative) current peak corresponds to the oxidation and removal of the previously deposited silver atoms. An enlarged view of the CV for the planar electrode (Figure 3 inset) clearly displays the well-defined features expected for Ag UPD on polycrystalline gold,[26] but these features are dwarfed by those of the NPGL electrodes when they are shown together. The integrated charge under these reduction and oxidation peaks varies directly with the available surface area of the electrodes.[27] Comparing the integrated charge for NPGL electrodes with dealloying times of 15 min, 1 h, 3 h, and 24 h to that obtained from a planar electrode revealed that the NPGL electrodes provided surface areas approximately 18.9, 11.6, 9.4, and 4.6 times greater than the flat electrode, respectively. This trend is consistent with the reduction in surface area resulting from the surface diffusion driven coarsening process that progresses as the leaf is exposed to nitric acid as described previously.[28] SEM images of NPGL electrodes after dealloying times of 15 min, 1 h, and 24 h are presented in Supporting Information.

Electrode Surface Modification and Characterization. To explore the extent to which the versatility of a planar gold electrode was retained by the NPGL electrodes, the surfaces of the latter were exposed to ethanolic so-

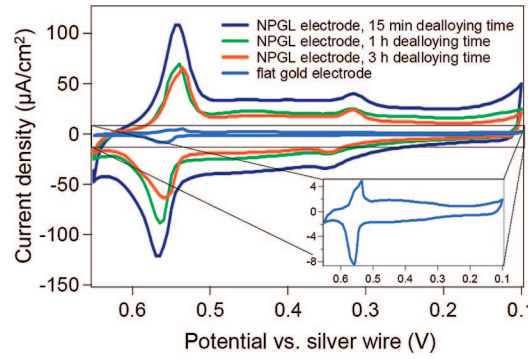

Figure 3. Cyclic voltammograms of NPGL electrodes after various dealloying times. Current peak areas decrease with longer dealloying times, indicating a reduction in surface area due to pore widening. Inset: Enlarged view of the CV for a planar electrode (control) to display well-defined features.

TABLE 1. Contact Angles and Electrochemical Properties of Modified NPGL Electrode Films[a]

NPGL surface modification	θ_a (degrees)	C_F (μF)	log R_{CT} (log Ω · cm^{-2})	W (Ω · cm^{-2})
bare NPGL	96 ± 1.4			214 ± 39
SC_8SAM	120 ± 2.8	2.57 ± 0.28	4.36 ± 0.15	
SC_{10}SAM	120 ± 3.0	2.25 ± 0.57	4.30 ± 0.20	
SC_{12}SAM	119 ± 3.8	1.46 ± 0.24	5.03 ± 0.47	
SC_{14}SAM	109 ± 4.1	1.34 ± 0.31	4.89 ± 0.35	
SC_{16}SAM	119 ± 5.8	1.19 ± 0.39	4.90 ± 0.10	
SC_{18}SAM	123 ± 3.9	1.08 ± 0.21	4.95 ± 0.36	
SC_2NH_2SAM	19 ± 4.9			201 ± 66
TPDA functionalized SAM	35 ± 6.3			215 ± 78
PSI immobilized	90 ± 2.8		0.90 ± 0.16	253 ± 63

[a]Reported values and errors reflect the mean and standard deviations of the measurements, respectively ($n \geq 3$ for each surface modification).

lutions containing ω-terminated alkyl thiols of interest to form of a variety of SAMs. Contact angles of water (θ_a) and several parameters obtained *via* electrochemical impedance spectroscopy (EIS) were measured to confirm the presence of the SAMs at the surface and throughout the mesoporous electrode film, respectively (Table 1). A series of methyl-terminated SAMs were formed on the NPGL surface and exhibited advancing water contact angles of 119−120°. These values are roughly 6−10° higher than those exhibited by the same SAMs on 2D surfaces, reflecting the effect of the roughness introduced by the mesoporous film on the contact angles as established by Wenzel.[29] Contact angles were generally consistent with the Wenzel equation in that those of hydrophobic and hydrophilic SAMs on NPGL were higher and lower, respectively, than the contact angles measured for the same SAMs on 2D surfaces. These values are consistent with the presence of the SAMs at the outer facets of the structures but do not necessarily reveal information about the extent of thiol adsorption within the pores.

In order to probe the surface properties throughout the porosity of the NPGL film, we obtained EIS spectra in the presence of $K_3Fe(CN)_6$ and $K_4Fe(CN)_6$ in 0.1 M Na_2SO_4. These data were collected for NPGL attached to glass supports to ensure that the measurements were representative of the NPGL film rather than the underlying gold surface (if an NPGL/Au electrode had been used). The *n*-alkanethiolate SAMs contributed a significant charge transfer resistance and a greatly reduced film capacitance as determined by fitting the spectra with a Randle's equivalent circuit model (figure in Supporting Information) to extract these parameters. Film capacitances (C_F) measured for these surfaces displayed a decreasing trend with increasing number of CH_2 units in the adsorbate, affirming an effective increase in film thickness for alkanethiolate SAMs of increasing chain length as previously demonstrated on a 2D surface.[30] Charge transfer resistance (R_{CT}) measurements displayed a relatively large variance with the -SC_8 and -SC_{10} SAMs exhibiting statistically lower resistances than those obtained for SAMs prepared from longer chain alkanethiols, which has also been reported for *n*-alkanethiolate SAMs on 2D surfaces.[30] In contrast to the barrier performance of the *n*-alkanethiolate films, NPGL surfaces modified with 2-aminoethanethiol and those further modified with terephthaldialdahyde (TPDA) (Figure 4a,b) exhibited impedances similar to a bare NPGL electrode. For these systems, the charge transfer resistance and the film capacitance contributions to impedance were much less significant than those exhibited by the alkanethiolate coatings, which caused the electrochemical impedance in these systems to be dominated by diffusion of the redox probes to the surface. These spectra were fit to a mixed kinetic and charge transfer equivalent circuit model which included a Warburg impedance (W) (Figure S1 in Supporting Information). The observation that the TPDA-functionalized monolayer introduces little impedance to charge transfer at the electrode surface is a characteristic result of the poorly packed 2-aminoethanethiolate precursor SAM.[31] The relative ease by which charge can transfer through the TPDA-modified SAM, combined with its ability to covalently bind exposed lysine residues of proteins, suggests its utility for applications involving electron transfer to PSI reaction centers.

Photosystem I Immobilization and Photocurrent Responses. To anchor PSI directly onto the electrode, the TPDA-functionalized surface was exposed to a phosphate-buffered solution containing PSI suspended in Triton X-100 surfactant. Accessible lysine residues on the outer portions of the protein bind covalently to the terminal aldehydic groups of the SAM,[32] anchoring the protein to the NPGL surface (Figure 4c).[33] The presence of PSI on the surface of the NPGL was evident by an increase in the contact angle from ~30° on the TPDA-modified surface to ~90° after the protein complex's immobilization. The reflectance−absorption infrared spectrum (RAIRS) of the PSI-modified NPGL (Figure 4d) clearly shows the characteristic Amide I and II bands at approximately 1664 and 1546 cm^{-1}, respectively, further confirming the presence of PSI on the electrode surface.[13] Immobilization of PSI also affects the EIS spectrum by introducing a measurable charge transfer resistance while still retaining Warburg impedance behavior

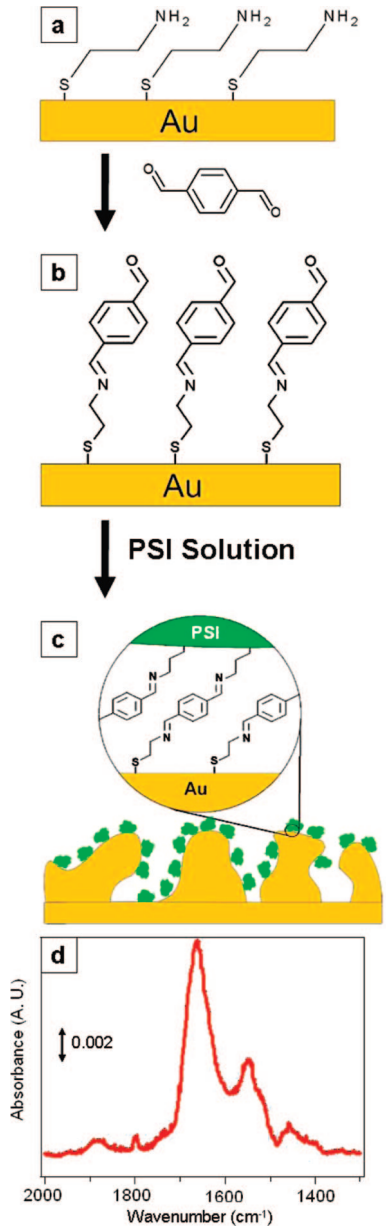

Figure 4. Photosystem I attachment scheme and RAIR spectrum of PSI-modified NPGL surface. (a) NPGL surface is modified by 2-aminoethanethiol. (b) Exposure to TPDA provides the surface with aldehydic terminal groups. (c) Exposed lysine residues on PSI covalently bind the protein complex to the electrode surface. (d) RAIR spectrum of PSI-modified NPGL surface; characteristic Amide I and II peaks are observed near 1667 and 1546 cm^{-1}, respectively.

of the TPDA-modified SAM precursor at low frequencies.

Photochronoamperometric measurements were taken for both electrodes in a phosphate buffer solution containing dichloroindophenol (DCIP) as an electrochemical mediator and sodium ascorbate (NaAs) as a sacrificial reagent. Upon irradiation, energy from incident photons is collected by chlorophylls oriented throughout the protein and transferred to the P700 reaction center within PSI. This energy causes the reaction center to achieve an excited state (denoted P700*), after which it initiates charge separation by promoting an electron to an elevated energy level. The excited electron leaves the P700 reaction center in an electron-deficient state (denoted $P700^+$) as it transfers across the protein complex to reduce the iron−sulfur complex F_B where the electron can be transferred to an electrochemical mediator in solution. In order for the process to begin again, the $P700^+$ reaction center must be reduced back to P700. When this reduction is achieved by electrons from the conduction band of the underlying gold substrate, a cathodic current response is measured by the potentiostat. The difference between the current measured when the system is dark and that measured when the electrode is irradiated is referred to as the photocurrent response of the cell. Typical photocurrent responses for PSI films attached to 2D electrodes and NPGL electrodes (3 h dealloying time) are shown in Figure 5a. The NPGL electrode displayed an enhancement in photocurrent of ~3-fold with respect to the 2D electrode due to the increased number density of PSI complexes bound to the porous substrate. The magnitude of this photocurrent enhancement for the NPGL electrode is not as great as the surface area enhancement determined by Ag UPD in the cyclic voltammetry experiment; this observation arises because the major axis of a PSI complex is comparable to the diameter of some of the smaller NPGL pores as previously mentioned, and if a PSI were to attach near such a pore, it could block potential binding sites deeper inside the cavity. Figure 5b shows photocurrent enhancements provided by PSI-modified NPGL electrodes of varying dealloying times, presented alongside the surface area enhancements determined by the UPD of silver. Although the greatest surface area enhancements are achieved at short dealloying times because of the relatively small pore sizes, these pores are too small to offer interior binding sites to the larger PSI complexes. At dealloying times of 1 h and longer, many of the pores are of adequate dimensions to accommodate multiple PSI complexes, resulting in an increase in the number of PSI complexes bound per unit of geometric area, thus producing photocurrent enhancements of roughly 3−7-fold with respect to the planar electrodes. Dealloying times of 24 h consistently produced electrodes with similar surface area and photocurrent enhancements, suggesting nearly all of the surface area introduced to the electrode by the NPGL film is accessible to PSI. In context of the previously reported photocurrent responses of 3−5 nA/cm^2 in 2007[34] and ~100 nA/cm^2 in 2008,[33] the ~300 nA/cm^2 response shown in Figure 5a realizes progress that spans 2 orders of magnitude in just 2 years.

Photocurrent Responses at Varying Light Intensities. The response of these electrodes to varying intensities of polychromatic visible light must be assessed should they be used in photocatalytic applications that utilize solar energy. As preliminary investigation of this behav-

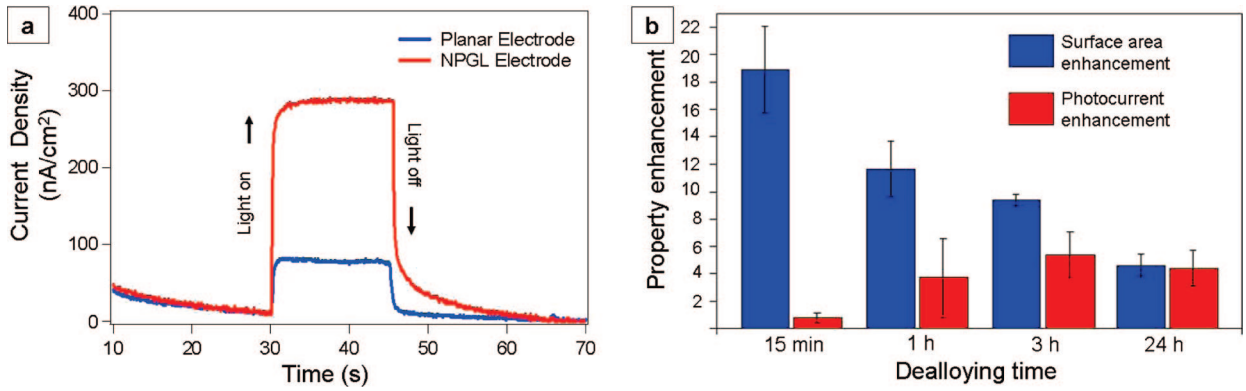

Figure 5. Photocurrent responses of PSI-modified NPGL electrodes. (a) Photochronoamperometric data for a planar gold electrode and an NPGL electrode (3 h dealloying time) using an illumination intensity of approximately 3.7 W/m^2 with a red filter. (b) Photocurrent and surface area enhancements provided by NPGL films of various dealloying times with respect to planar gold electrodes. Mean values are reported, and the standard deviations are shown as error bars. Although large surface area enhancements are achieved at short dealloying times, the pore sizes are too small to allow multiple PSI complexes to attach inside the pores. Dealloying times of 3 h and longer yield electrodes whose surface area and photocurrent enhancements are similar in magnitude, suggesting that the majority of the surface area is accessible to PSI ($n \geq 3$ for planar and NPGL electrodes at each dealloying time).

ior, PSI-modified planar and NGPL electrodes (1 h dealloying time) were irradiated with several different intensities of white light. The intensity at the surface of the electrode was measured with a light meter, and the corresponding photocurrent response was recorded. This experiment was repeated for three identically prepared NPGL samples and four identically prepared planar samples, and the results are presented in Figure 6. Representative photochronoamperometry data from individual samples are included in Supporting Information.

These photocurrent responses display an increasing trend with light intensity, indicating that the photocurrents observed over this range of intensities not only are influenced by the kinetics governing the interaction of PSI's electron-donating and -accepting reaction centers with the electrochemical mediators and the underlying electrode but also are largely dependent upon the rate of photoexcitation of P700 reaction centers.

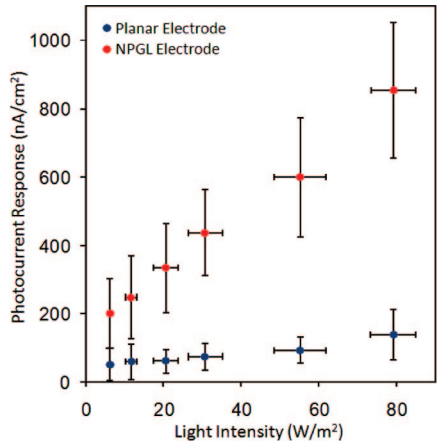

Figure 6. Photocurrent responses at various intensities of white light. Points represent mean values, with vertical and horizontal error bars showing the standard deviations of the photocurrent responses and light intensities, respectively, measured at six different lamp intensity settings ($n = 3$ for NPGL electrodes, $n = 4$ for planar electrodes).

As stated by the Beer–Lambert Law, absorbance varies directly with the concentration of the absorbing species, thus the relatively sharp response to increasing light intensities by PSI adsorbed onto the NPGL films is consistent with the larger PSI/electrode interfacial areas, which effectively raises the protein's concentration per geometric area, allowing for increased light absorption and photocurrent production. These results also demonstrate that the photocurrent enhancements provided by the NPGL electrode films are preserved over the range of intensities employed in this study.

CONCLUSIONS

In summary, we have presented a method to fabricate nanoporous gold leaf electrode films, attach them to gold and glass supports, and impart photonic energy conversion capabilities to them by modification with Photosystem I. We have demonstrated that the average feature size and hence surface area of these NPGL electrodes can be adjusted, and that they can be modified by various SAMs to exhibit different electrochemical behaviors and surface properties. The immobilization of PSI on the surface of NPGL electrodes in comparison to planar electrodes provided an increase in PSI-catalyzed photocurrent in the presence of electrochemical mediators. The photocurrents produced by these electrodes were dependent upon both intensity of light irradiating the electrodes and the dealloying times used during the electrodes' fabrication, with dealloying times of 3 h and longer producing feature sizes that render the majority of the surface area accessible to PSI. The robust electrode fabrication method presented herein can easily be extended to a myriad of applications beyond those described in this work, making 3D mesoporous surfaces readily available through straightforward, benchtop laboratory techniques.

MATERIALS AND METHODS

Gold Leaf Dealloying. One hundred nanometer thick Monarch 12 Karat white gold (fineartstore.com) was cut to ~1.5 × 1.5 cm and floated on approximately 40 mL of concentrated nitric acid (Fisher) in a 50 mL glass beaker for various dealloying times to yield NPGL. Au/Si supports were prepared by thermally evaporating 125 nm of Au (J&J Materials) onto silicon wafers (Montico Silicon, <100> orientation, 100 mm diameter, 500−550 mm thick) with a 10 nm adhesion layer of Cr (R.D. Mathis). Samples were cut to approximately 1.3 cm × 2 cm. The gold surface was then exposed to a 20 mM solution of hexanedithiol (Aldrich) in ethanol (Pharmco, AAPER) for 24 h. Glass supports were prepared by exposing glass microscope slides (Fisher) to a 5 mM solution of mercaptopropyltrimethoxysilane (Acros) in hexane (Fisher) at 60 °C for 1 h. NPGL was then collected on the surface of the substrates as shown in Figure 1 and described in the discussion of the fabrication process in this paper.

Scanning Electron Microscopy. SEM images were taken with a Hitachi S-4200 scanning electron microscope using an accelerating voltage of 15 kV.

Cyclic Voltammetry. Cyclic voltammetry was performed with a Gamry Instruments CMS300 electrochemical system using an aqueous solution of 0.1 M sulfuric acid (EMD) and 0.6 mM silver sulfate (Aldrich) with a Ag/AgCl reference and a gold counter electrode. Voltage was cycled from 0.65 to 0.05 V with a scan rate of 20 mV/s. The fourth cycle is presented in this work.

SAM Formation, TPDA Modification, and PSI Immobilization. SAMs on gold surfaces were formed by exposing the electrode surface to 1 mM ethanolic solutions of the thiol adsorbate for 12 h; samples used in the EIS analysis were exposed at least 50 h to allow ample time to reduce the density of defect sites within the monolayer. Octanethiol, decanethiol, dodecanethiol, hexadecanethiol, and octadecanethiol were purchased from Aldrich; tetradecanethiol was purchased from Fluka; aminoethanethiol was purchased from Acros. Amine-terminated SAMs on NPGL were modified with TPDA by exposing the surface to 1 mM solutions of terephthaldialdehyde (Aldrich) for 1 h. PSI attachment was accomplished by exposing the TPDA-modified surface to a solution of approximately 1.5×10^{-7} mol L^{-1} of PSI, as measured by P700 content, in elution buffer (0.2 M Na phosphate, 0.05 wt/vol % Triton X-100) for 48−72 h at 4 °C, after which, the samples were rinsed with deionized water and dried with nitrogen.

Contact Angle Measurements. Advancing contact angles of deionized water were measured using a Rame-Hart goniometer. Three measurements were taken on different locations for at least two independently prepared samples. Reported values and errors reflect the mean and standard deviations of the measurements, respectively.

Electrochemical Impedance Spectroscopy. EIS was performed with a Gamry Instruments CMS300 impedance system using electrochemical cell consisting of 1 mM $K_3Fe(CN)_6$ and 1 mM $K_4Fe(CN)_6$ in 0.1 M Na_2SO_4(aq) as an electrolyte, a Ag/AgCl reference electrode, a gold counter electrode, and the sample of interest as the working electrode. The frequency of a 10 mV rms AC voltage was varied from 10^{-1} to 10^5 Hz, with 10 points per decade recorded. Data were fit to equivalent circuit models using the Gamry E-chem Analyst software package. Reported values and errors reflect the mean and standard deviations, respectively, of at least three independently prepared samples.

PSI Extraction. Commercial baby spinach leaves were used for the isolation of thylakoid membranes by the method of Reeves and Hall[35] with modifications as described recently.[36] A hydroxylapatite column was used for additional separation and isolation of native PSI involved as described by Shiozawa *et al.*[37] and Lee *et al.*[38] The effluent PSI suspension was stored at −80 °C. The P700 reaction center concentration of the elution buffer used in this study was determined to be approximately 9 μM by monitoring the changes in UV−vis absorbance as described by Baba *et al.*[39]

Reflectance−Absorption Infrared Spectroscopy. RAIRS was performed with a Bio-Rad Excalibur FTS-3000 infrared spectrometer, using p-polarized light at an incident angle approximately 80° from the surface normal. The instrument was operated in single reflection mode. One thousand scans were accumulated for each sample, using a sample of bare NPGL attached to a gold substrate as a background. A water spectrum was subtracted from that spectrum obtained from the PSI-modified NPGL, and the difference is presented in this work.

Photochronoamperometry. Photochronoamperometric data were collected using a CH Instruments CHI660a electrochemical workstation with a Faraday cage. A three-electrode cell was used with the PSI-modified NPGL as the working electrode, platinum mesh as the counter electrode, and Ag/AgCl as the reference electrode. Planar PSI-modified Au electrodes were prepared identically and served as working electrodes in order to calculate photocurrent enhancements contributed by the NPGL. All photochronoamperometric data were taken at a bias of −0.1 V *vs* Ag/AgCl, in a mediator solution consisting of 250 μM dichloroindophenol (Acros), 5 mM sodium ascorbate (Alrich), and 100 mM NaCl (Fisher) in a pH 7 phosphate buffer (Fisher). The electrodes were illuminated with a Gebrauch KL 2500 LCD lamp. Light intensity was measured using a SPER Scientific 840022 advanced light meter.

Supporting Information Available: Additional supporting figures. This material is available free of charge *via* the Internet at http://pubs.acs.org.

REFERENCES AND NOTES

1. He, W. Z.; Malkin, R. Photosystems I and II. In *Photosynthesis: A Comprhensive Treatise*; Raghavendra, A. S., Ed.; Cambridge University Press: Cambridge, 1998; pp 29−43.
2. Alivisatos, P.; Cummings, P.; Yoreo, J. D.; Fichthorn, K.; Gates, B.; Hwang, R.; Lowndes, D.; Majumdar, A.; Makowski, L.; Michalske, T. *et al. Nanoscience Research for Energy Needs: Report of the National Nanotechnology Initiative Grand Challenge Workshop*; The National Nanotechnology Coordination Office: Arlington, 2004.
3. Lee, J. W.; Collins, R. T.; Greenbaum, E. Molecular Ionic Probes: A New Class of Hill Reagents and their Potential for Nanofabrication and Biometallocatalysis. *J. Phys. Chem. B* **1998**, *102*, 2095–2100.
4. Das, R.; Kiley, P. J.; Segal, M.; Norville, J.; Yu, A. A.; Wang, L. Y.; Trammell, S. A.; Reddick, L. E.; Kumar, R.; Stellacci, F. Integration of Photosynthetic Protein Molecular Complexes in Solid-State Electronic Devices. *Nano Lett.* **2004**, *4*, 1079–1083.
5. Frolov, L.; Rosenwaks, Y.; Carmeli, C.; Carmeli, I. Fabrication of a Photoelectronic Device by Direct Chemical Binding of the Photosynthetic Reaction Center Protein to Metal Surfaces. *Adv. Mater.* **2005**, *17*, 2434–2437.
6. Frolov, L.; Wilner, O.; Carmeli, C.; Carmeli, I. Fabrication of Oriented Multilayers of Photosystem I Proteins on Solid Surfaces by Auto-Metallization. *Adv. Mater.* **2008**, *20*, 263–266.
7. Carmeli, I.; Frolov, L.; Carmeli, C.; Richter, S. Photovoltaic Activity of Photosystem I-Based Self-Assembled Monolayer. *J. Am. Chem. Soc.* **2007**, *129*, 12352–12353.
8. Carmeli, I.; Mangold, M.; Frolov, L.; Zebli, B.; Carmeli, C.; Richter, S.; Holleitner, A. W. A Photosynthetic Reaction Center Covalently Bound to Carbon Nanotubes. *Adv. Mater.* **2007**, *19*, 3901–3905.
9. Terasaki, N.; Yamamoto, N.; Hiraga, T.; Sato, I.; Inoue, Y.; Yamada, S. Fabrication of Novel Photosystem I−Gold Nanoparticle Hybrids and their Photocurrent Enhancement. *Thin Solid Films* **2006**, *499*, 153–156.
10. Terasaki, N.; Yamamoto, N.; Tamada, K.; Hattori, M.; Hiraga, T.; Tohri, A.; Sato, I.; Iwai, M.; Iwai, M.; Taguchi, S.; *et al.* Bio-Photo Sensor: Cyanobacterial Photosystem I Coupled with Transistor *via* Molecular Wire. *Biochim. Biophys. Acta* **2007**, *1767*, 653–659.
11. Laibinis, P. E.; Palmer, B. J.; Lee, S.-W.; Jennings, G. K. In *Thin Films*; Academic Press: Boston, 1998; pp 1−41.
12. Lee, I.; Lee, J. W.; Greenbaum, E. Biomolecular Electronics: Vectorial Arrays of Photosynthetic Reaction Centers. *Phys. Rev. Lett.* **1997**, *79*, 3294–3297.
13. Kincaid, H. A.; Niedringhaus, T.; Ciobanu, M.; Cliffel, D. E.; Jennings, G. K. Entrapment of Photosystem I within Self-Assembled Films. *Langmuir* **2006**, *22*, 8114–8120.

14. Huang, W. X.; Kim, J. B.; Bruening, M. L.; Baker, G. L. Functionalization of Surfaces by Water-Accelerated Atom-Transfer Radical Polymerization of Hydroxyethyl Methacrylate and Subsequent Derivatization. *Macromolecules* **2002**, *35*, 1175–1179.
15. Jennings, G. K.; Brantley, E. L. Physicochemical Properties of Surface-Initiated Polymer Films in the Modification and Processing of Materials. *Adv. Mater.* **2004**, *16*, 1983–1994.
16. Berron, B. J.; Greaybill, E. P.; Jennings, G. K. Growth and Structure of Surface-Intitated Poly(*n*-alkylnorbornene) Films. *Langmuir* **2007**, *23*, 11651–11655.
17. Sun, T. L.; Wang, G. J.; Feng, L.; Liu, B. Q.; Ma, Y. M.; Jiang, L.; Zhu, D. B. Reversible Switching Between Superhydrophilicity and Superhydrophobicity. *Angew. Chem., Int. Ed.* **2004**, *43*, 357–360.
18. Martin, C. R. Nanomaterials: A Membrane-Based Synthetic Approach. *Science* **1994**, *266*, 1961–1966.
19. Sander, M. S.; Tan, L. S. Nanoparticle Arrays on Surfaces Fabricated Using Anodic Alumina Films as Templates. *Adv. Funct. Mater.* **2003**, *13*, 393–397.
20. Wirtz, M.; Martin, C. R. Template-Fabricated Gold Nanowires and Nanotubes. *Adv. Mater.* **2003**, *15*, 455–458.
21. Prikulis, J.; Hanarp, P.; Olofsson, L.; Sutherland, D.; Kall, M. Optical Spectroscopy of Nanometric Holes in Thin Gold Films. *Nano Lett.* **2004**, *4*, 1003–1007.
22. Turkevich, J.; Stevenson, P. C.; Hillier, J. A Study of the Nucleation and Growth Processes in the Synthesis of Colloidal Gold. *Discuss. Faraday Soc.* **1951**, *11*, 55–75.
23. Ding, Y.; Kim, Y. J.; Erlebacher, J. Nanoporous Gold Leaf: "Ancient Technology" Advanced Material. *Adv. Mater.* **2004**, *16*, 1897–1900.
24. Erlebacher, J.; Aziz, M. J.; Karma, A.; Dimitrov, N.; Sieradzki, K. Evolution of Nanoporosity in Dealloying. *Nature* **2001**, *410*, 450–453.
25. Amunts, A.; Drory, O.; Nelson, N. The Structure of a Plant Photosystem I Supercomplex at 3.4 Angstrom Resolution. *Nature* **2007**, *447*, 58–63.
26. Chen, C. H.; Vesecky, S. M.; Gewirth, A. A. *In Situ* Atomic Force Microscopy of Underpotential Deposition of Silver on Gold(111). *J. Am. Chem. Soc.* **1992**, *114*, 451–458.
27. Myland, J. C.; Oldham, K. B. Quasireversible Cyclic Voltammetry of a Surface Confined Redox System: A Mathematical Treatment. *Electrochem. Commun.* **2005**, *7*, 282–287.
28. Erlebacher, J. An Atomistic Description of Dealloying. *J. Electrochem. Soc.* **2004**, *151*, C614–C626.
29. Wenzel, R. N. Resistance of Solid Surfaces to Wetting by Water. *Ind. Eng. Chem.* **1936**, *28*, 988–994.
30. Jennings, G. K.; Munro, J. C.; Yong, T. H.; Laibinis, P. E. Effect of Chain Length on the Protection of Copper by *n*-Alkanethiols. *Langmuir* **1998**, *14*, 6130–6139.
31. Wallwork, M. L.; Smith, D. A.; Zhang, J.; Kirkham, J.; Robinson, C. Complex Chemical Force Titration Behavior of Amine-Terminated Self-Assembled Monolayers. *Langmuir* **2001**, *17*, 1126–1131.
32. Rozkiewicz, D. I.; Ravoo, B. J.; Reinhoudt, D. N. Reversible Covalent Patterning of Self-Assembled Monolayers on Gold and Silicon Oxide Surfaces. *Langmuir* **2005**, *21*, 6337–6343.
33. Faulkner, C. J.; Lees, S.; Ciesielski, P. N.; Cliffel, D. E.; Jennings, G. K. Rapid Assembly of Photosystem I Monolayers on Gold Electrodes. *Langmuir* **2008**, *24*, 8409–8412.
34. Ciobanu, M.; Kincaid, H. A.; Lo, V.; Dukes, A. D.; Jennings, G. K.; Cliffel, D. E. Electrochemistry and Photoelectrochemistry of Photosystem I Adsorbed on Hydroxyl-Terminated Monolayers. *J. Electroanal. Chem.* **2007**, *599*, 72–78.
35. Reeves, S. G.; Hall, D. O. Higher Plant Chloroplasts and Grana: General Preparative Procedures (Excluding High Carbon Dioxide Fixation Ability Chloroplasts). *Methods Enzymol.* **1980**, *69*, 85–94.
36. Ciobanu, M.; Kincaid, H. A.; Jennings, G. K.; Cliffel, D. E. Photosystem I Patterning Imaged by Scanning Electrochemical Microscopy. *Langmuir* **2005**, *21*, 692–698.
37. Shiozawa, J. A.; Alberte, R. S.; Thornber, J. P. P700-Chlorophyll *a*-Protein—Isolation and Some Characteristics of Complex in Higher Plants. *Arch. Biochem. Biophys.* **1974**, *165*, 388–397.
38. Lee, J. W.; Zipfel, W.; Owens, T. G. Quenching of Chlorophyll Excited-States in Photosystem-I by Quinones—Stern−Volmer Analysis of Fluorescence and Photochemical Yield. *J. Lumin.* **1992**, *51*, 79–89.
39. Baba, K.; Itoh, S.; Hastings, G.; Hoshina, S. Photoinhibition of Photosystem I Electron Transfer Activity in Isolated Photosystem I Preparations with Different Chlorophyll Contents. *Photosynth. Res.* **1996**, *47*, 121–130.